TOMOGRAPHY® RESEARCH ARTICLE

A Radiodensity Histogram Study of the Brain in Multiple Sclerosis

Keith A. Cauley[1] and Samuel W. Fielden[1,2]

[1]Department of Radiology, Geisinger Medical Center, Danville, PA; and [2]Department of Imaging Science & Innovation, Geisinger Health System, Lewisburg, PA

Corresponding Author:
Keith A. Cauley, MD
Department of Radiology, Geisinger Medical Center, Danville, PA USA 17821;
E-mail: keithcauley@hotmail.com

Key Words: Computed tomography, radiodensity, histogram, multiple sclerosis
Abbreviations: Multiple sclerosis (MS), magnetic resonance imaging (MRI), computed tomography (CT), normal-appearing brain tissue (NABT), normal-appearing white matter (NAWM), Expanded Disability Status Scale (EDSS), receiver operating characteristic (ROC), area under the ROC curve (AUC)

ABSTRACT

Multiple sclerosis (MS) is a progressive neurodegenerative disease, affecting 1 million Americans and 2.5 million people globally. Although the diagnosis is made clinically, imaging plays a major role in diagnosing and monitoring disease progression and treatment response. Magnetic resonance imaging (MRI) has proven sensitive in imaging MS lesions, but the characterization offered by routine clinical MRI remains qualitative and with discrepancies between imaging and clinical findings. We investigated the ability of digital analysis of noncontrast head computed tomography (CT) images to detect global brain changes of MS. All routine diagnostic head CTs obtained on patients with known MS obtained from 1 of 2 scan platforms from 6/1/2011 to 6/1/2015 were reviewed. Head CT images from 54 patients with MS met inclusion criteria. Head CT images were processed and histogram metrics were compared to age- and gender- matched control subjects from the same CT scanners during the same time interval. Histogram metrics were correlated with plaque burden as seen on MRI studies. Compared with control subjects, patients had increased total brain radiodensity ($P < .0001$), further characterized as an increased histogram modal radiodensity ($P < .0001$) with decrease in histogram skewness ($P < .0001$). Radiodensity decreased with increasing plaque burden. Similar findings were seen in the patients with only mild plaque burden sub- group. Radiodensity is a unique tissue metric that is not measured by other imaging techniques. Our study finds that brain radiodensity histogram metrics highly correlate with MS, even in cases with minimal plaque burden.

INTRODUCTION

Numerous studies have shown that multiple sclerosis (MS) entails global changes to the normal-appearing brain tissue (NABT), as assessed with diffusion-weighted imaging (1, 2), nonconventional magnetic resonance (MR) techniques such as T1 and T2 relaxation time mapping (3-5), and diffusion tensor imaging (6). Although lacking the contrast and the multisequential capabilities of MR, computed tomography (CT) offers a calibrated measurement of radiodensity, the Hounsfield unit (HU), a tissue metric unique to this modality. We wished to investigate whether the global changes of MS that have been seen with MRI could be detected by digital analysis of the brain CT radiodensity histogram. Such a calibrated metric could offer a quantitative assessment of global brain tissue changes in MS. We hypothesized that MS brain tissue would have abnormal radiodensity as reflected in the brain radiodensity histogram.

METHODS

Study Design

As prospective studies involving CT imaging would involve radiation exposure, this pilot study was limited to a retrospective analysis of head CTs performed on patients with MS that were identified from the PACS (picture archiving and communication system) imaging archive. The study was approved by this institution's review board, and waiver of consent was granted.

Cases were identified by a search of the imaging database by cross-referencing the ICD-10 code for MS (G35), and head CT imaging from the individual CT scan platform. To increase the cohort size and verify that findings were independent of scanner cohort and scanner platform, cases were reviewed from 2 different CT scanners over a 5-year period (6/1/2011 to 6/1/2016). Clinical indications for CT of patients with MS were 'trauma' without traumatic findings or general worsening of symptoms (weakness, visual or mental status changes). Cases with acute or chronic findings other than white matter changes of MS (skull fracture, intracranial hemorrhage, stroke, etc.) were not included. Cases with current use of steroids (2 cases) were also excluded. As described below, cases where the plaque burden could not be unequivocally established were not included.

Age- and gender-matched control subjects were clinical cases from the same scan platform over the same time period.

ISSN 2379-1381 http://dx.doi.org/10.18383/j.tom.2018.00050

Table 1. Summary of Patient Clinical Data for Patients Scanned in Scanner 1

	Mean	SD	Range
Controls (n = 39)	30 F, 9 M		
Age (years)	50.7	16.1	26–78
Total MS (n = 39)			
Gender	30 F, 9 M		
Age (year)	53.6	10.5	29–82
Disease duration (years)	12.1	8.0	0.25–>20
EDSS	5.3	2.3	2–9
Mild MS (n = 16)			
Gender	14 F, 2 M		
Age (year)	50.5	11.5	29–76
Disease duration (years)	7.42	8	0.25–>20
EDSS	4.0	2.0	2–9
Moderate MS (n = 16)			
Gender	11 F, 5 M		
Age (year)	51.7	15.6	33–82
Disease duration (years)	13.9	6.9	<1–>20
EDSS	6.1	1.9	3–9
Severe MS (n = 7)			
Gender	5 F, 2 M		
Age (year)	56.1	6.5	51–67
Disease duration (years)	>19	2	15–>20
EDSS	6.2	2.5	2–8.5
Disease course	RRMS (3) PPMS (1) SPMS (4) PMS-NOS (2) NMO (2) MS-NOS (29)		
Disease-modifying agent	16 of 39 patients were using a disease-modifying agent (glatiramer acetate, teriflunomide, delfampridine) at the time of the CT scan		

Summary of patient data for scanner 2 is provided as online supplementary data. Abbreviations are discussed in the Results section of the text.

Control cases were scanned for nonspecific symptoms (headache, syncope, vertigo), were without known systemic disease, and were discharged without incident. All control cases were interpreted as "normal" (without acute or chronic abnormal findings) by 2 board-certified neuroradiologists. In total, 54 patients with a clinically confirmed diagnosis of MS met inclusion criteria, and 54 patients with normal head CT scans were the subjects of this study.

A thorough clinical record review was conducted to learn the details of diagnosis, disease duration, medical treatments, and clinical status of patients with MS at the time of the CT scan (scanner 1, Table 1; scanner 2, online supplemental Table S1). All cases were clinically established MS or MS variant. Expanded Disability Status Scale (EDSS) was based on the clinical neurology notes at the time of the CT scan. Clinical review also showed the total numbers of gadolinium-enhanced MRI studies the patient had undergone.

Plaque burden was graded on the basis of brain MRI studies. MRI studies were performed either within 1 year of the CT scan or before and after the CT scan such that the plaque burden could be unequivocally deduced. If the plaque burden could not be reliably deduced, the study was not included. Semiquantitative plaque burden scaling was similar to that previously described (7); however, the 5 classes were simplified to 3—mild, moderate, and severe—as determined by a board-certified neuroradiologist (kac) (Figure 1). Mild plaque burden included a few nonspecific white matter changes to lesions, clearly suggesting MS. Moderate plaque burden included cases with typical MS plaques, but no large areas of confluence and without obvious callosal atrophy. Severe plaque burden included confluent white matter changes and diffuse callosal volume loss.

Imaging Methods

To minimize the possible contribution of variations in scanners and scanner calibration, studies from the 2 scanners were analyzed separately. Further, 39 MS cases that met inclusion criteria were from scanner 1 and 15 from scanner 2. Scanner 1 primarily serves the emergency department of a level I trauma center, and scanner 2 serves the emergency department of a level II trauma center. Both scanners are Toshiba Aquilon64 with helical acquisition and head CT protocol with 135 kVp and modulated MA, minimum 50 and maximum 290 mA, rotation time 0.75 seconds. Daily QA/QC studies for the scanner of interest conducted from June 2011 to June 2015 were retrospectively reviewed. HU of water and of a density phantom were recorded daily. Drift or trending was rarely observed. In a typical month (August 2011)

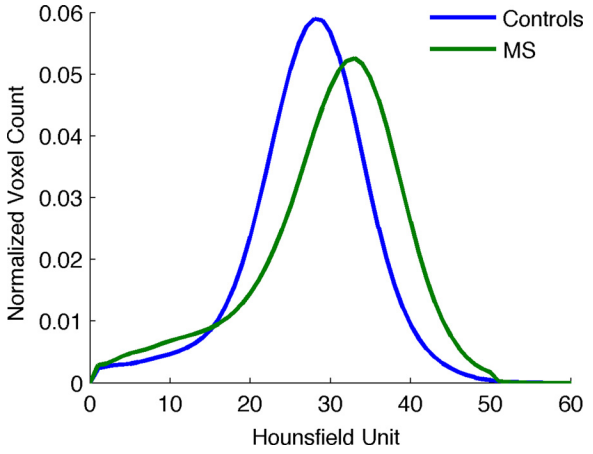

Figure 1. Population histograms. Brain computed tomography (CT) histogram of 39 patients with MS and 39 age- and gender-matched control subjects, scanned on the same imaging platform over the same time interval. A similar profile was seen for scanner 2.

for scanner 1, the HU of water varied between −1.1 and 1.8, mean 0.50, SD 0.071, tissue density plug from 93.3 to 95.2, mean 94.17, and SD 0.56. For scanner 2, the HU of water varied from −2.4 to 1.4, mean −0.16, SD 0.95, tissue density plug from 94.3 to 97.6, mean 95.77, and SD 0.85. In addition, scanners undergo an annual inspection by a medical physicist using the ACR phantom, and service engineers routinely test the calibration at preventive maintenance. Although the 2 different scanners are identical in terms of hardware and image acquisition protocol, pooling of the data would make the assumption that the calibrations and offsets are identical, which may not be the case. Therefore the data were processed separately.

Image Processing and Analysis

Images were thresholded, brain-extracted and segmented in FSL (FMRIB software library, Centre for Functional MRI of the Brain, Oxford, UK; www.fmrib.ox.ac.uk/fsl) (8-10) as described (11). The upper threshold value was set at 50 HU based on the prebrain-extracted histogram, and served to eliminate the skull. FSL BET standard brain extraction was used with fractional intensity threshold of 0.01 (10). FSL FAST was used to generate the image intensity inhomogeneity-corrected data set, which was used for all calculations. All cases were carefully reviewed for integrity of brain extraction.

Histograms and histogram analysis were performed in Matlab (release 2009b, the MathWorks, Inc., Natick, MA). Population histograms were generated as follows.

Histograms were normalized by voxel count. For the MS population histogram (Figure 2), all MS cases from scanner 1 (Table 1) are included (39 cases: female, 30; male, 9; average age, 50.7 years, SD = 16.1 years, range = 26–78 years). Further, 39 control subjects from the same time period and the same scanner were selected for age and gender (female, 30; male, 9; average age, 50.7 years, SD = 16.1 years, range = 26–79 years).

For histograms reflecting plaque burden (Figure 1), 16 cases of "mild" (female, 14; male, 2; average age, 50.5 years, SD = 11.5 years, range = 29–77 years), 16 cases of "moderate" burden were selected (female, 11; male, 5; average age, 51.7 years, SD = 15.6 years, range = 33–82 years). The 7 cases of severe plaque burden made up the "severe" histogram (female, 5; male, 2; average age, 56.1 years, SD = 6.5, range = 51–67 years).

The histogram of a normal brain CT follows the general appearance of the normal distribution. Matlab functions *skewness* and *kurtosis* were used to assess how far from this distribution each imaging data set lies. In Matlab, the skewness of a distribution is defined as $s = E(x - \mu)^3/\sigma^3$, where μ is the mean of x, σ is the standard deviation of x, and $E(t)$ represents the expected value of the quantity "t." Kurtosis is defined as $k = E(x - \mu)^4/\sigma^4$, where μ is the mean of x, σ is the standard

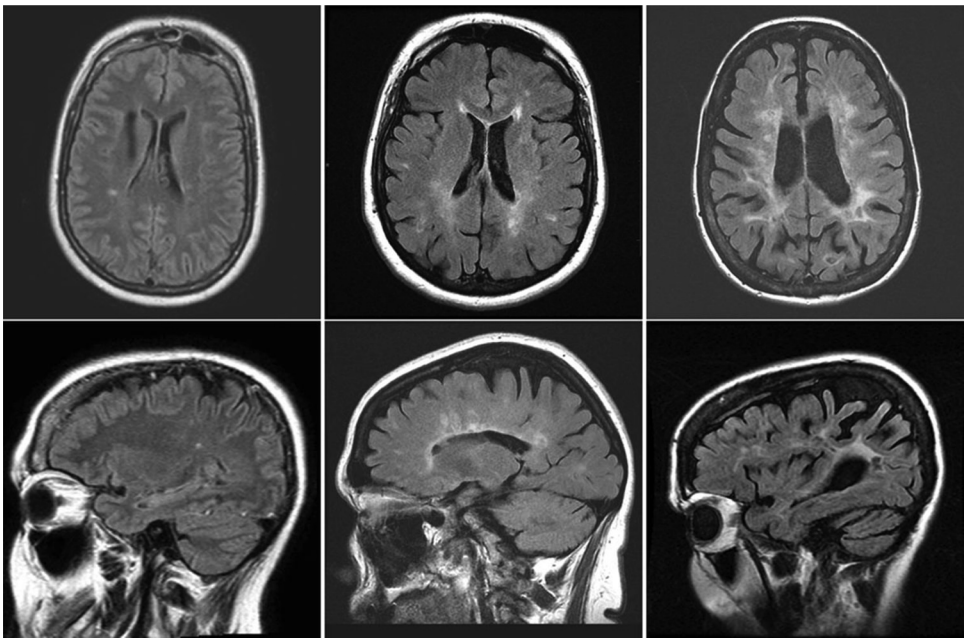

Figure 2. Magnetic resonance (MR) FLAIR images illustrating lesion load, "mild," "moderate," and "severe". Lower series with parasagittal FLAIR imaging.

deviation of x, and $E(t)$ represents the expected value of the quantity "t." The kurtosis of the normal distribution is "3." Other histogram features, including histogram mean, mode, full-width-at-half-maximum (FWHM), and standard deviation, were recorded.

To investigate regional differences in radiodensity, head CTs were brain-extracted as previously described. As coregistration of CT images to a reference image results in disruption of the voxel-wise integrity of the radiodensity, the MNI152 structural atlas was coregistered to each brain-extracted CT image, and each of the 9 masks was used to mask the head CT. A 10th mask was created as the difference between the total brain volume and the 9 brain regions (Figure 7, upper panel), and it represented the white matter. Each coregistration was visually inspected.

Statistical Analysis

Curve fitting and statistical analysis were performed using GraphPad Prism version 7.0c for Mac OS X (GraphPad Software, La Jolla California, www.graphpad.com). Box and whiskers plots show minimum, maximum, median, and quartile distribution of the data. Statistical significance was determined using the Kruskal–Wallis H nonparametric analysis of multiple groups, with significance at $P < .05$. Receiver operating characteristic (ROC) curves were generated in SPSS (IBM Corp released 2013. IBM Statistics for Mac Version 22.0, Armonk, NY).

RESULTS

A population histogram of all MS cases from scanner 1 (39 cases) and 39 age- and gender-matched control subjects shows that the MS histogram has an overall shift of the peak mode to the right (Figure 2). The histogram is slightly broader, and there is skewed appearance with a left-ward "tail" relative to the control histogram.

Patient demographics are shown in Table 1. EDSS: Expanded Disability Status Scale (12). Disease course: RRMS: relapsing remitting MS, PPMS: primary progressive MS, SPMS: secondary progressive MS, P-NOS: progressive MS not otherwise specified. The remainder of the cases were MS, not otherwise specified (NOS). Disease duration is estimated from symptom onset.

Patient clinical status was investigated through a thorough retrospective review of clinical data. The EDSS was estimated from a review of the clinical notes. The EDSS was significantly lower for the "mild" plaque burden group than for the "moderate" group ($P = .0273$), but other group differences did not prove significant ($P > .05$). Comorbidities in our study group (obesity, diabetes, coronary artery disease, degenerative arthritis) likely lower the accuracy of the EDSS, thus emphasizing mobility in evaluation of MS disability. Qualitative classification of plaque burden based on MRI studies showed that increasing plaque burden correlated with increasing patient age, increasing disease duration, and increasing EDSS score (Table 1).

Data from two different scan platforms served to increase the cohort size and to aid investigation of the reproducibility between platforms. To further investigate the differences in total brain radiodensity, and to address age as a possible covariable, a scatter plot of brain radiodensity versus age included patients with MS and control subjects from each scanner (Figure 3). The plot shows overall higher brain radiodensity in MS (Figure 3 and Table 2). Metrics of the scatter plots are summarized in Table 3.

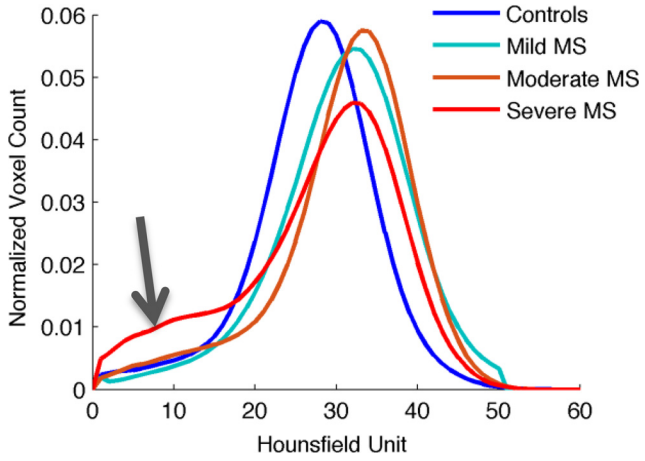

Figure 3. Head CT population histograms. Control subjects and patients with MS with mild, moderate, and severe plaque burden. Although the histogram modes are very similar, heavier plaque burden is characterized by a leftward (negative) skewness (arrow) as lesions are of decreased radiodensity. This results in a decreased mean radiodensity (see also Figure 5).

For scanner 1, there is a small but statistically significant decline in radiodensity of the brain in control subjects (Pearson $r = -0.502$, $P = .001$). The age-related decrease is less evident in the MS cases, which show greater scatter (Pearson $r = -0.133$, $P = .418$). For scanner 2, the correlations were not significant (Pearson $r = -0.064$, $P = .822$ for the control group, and $r = -0.131$, $P = .642$ for the MS group). The control subject age grouping was selected to match the MS patient age grouping for each scanner. The difference in the age dependence between the scanners can be attributed to a difference between the age clustering, as scanner 1 included a small cohort of older (>70 years) patients, whereas scanner 2 did

Table 2. Summary of Scatter Plot Statistics (Figure 3)

Mean Radiodensity (HU)		STD
Scanner 1		
Control (n = 39)	27.24	1.41
MS (n = 39)	30.24	2.37
All cases (n = 78)	28.74	2.46
Scanner 2		
Control (n = 15)	26.90	1.07
MS (n = 15)	29.61	2.16
All cases (n = 30)	28.26	2.17

Table 3. Significance of Differences Shown in the Box and Whisker Plot (Figure 5)

	Control	Mild	Mod		Control	Mild	Mod
Density (Mean)				Density (Mode)			
Total MS	<0.0001****			Total MS	<0.0001****		
Mild	<0.0001****			Mild	0.0432*		
Moderate	<0.0001****	>0.9999		Moderate	>0.0020**	>0.9999	
Severe	>0.9999	0.0212*	.0453*	Severe	>0.5558	>0.9999	>0.9999
Density (FWHM)				Density (Skewness)			
Total MS	>0.9999			Total MS	<0.0001****		
Mild	>0.9999			Mild	0.0022*		
Moderate	>0.9999	>0.9999		Moderate	<0.0001****	.3637	
Severe	>0.9999	>0.9999	>0.9999	Severe	>0.9999	>0.9999	.0648
Density (Kurtosis)				Density (Std)			
Total MS	>0.9999			Total MS	0.0010**		
Mild	0.0481*			Mild	>0.9999		
Moderate	>0.9999	0.6850		Moderate	0.0001***	.0024**	
Severe	0.0181*	<0.0001****	0.0115*	Severe	<0.0001****	0.0010***	>0.9999

Kruskal-Wallis H test was used with signficance at $P < .05$. Asterisks reflect degree of significance: ns, $P > 0.05$; *$P \leq 0.05$; **$P < 0.01$; ***$P < 0.001$; ****$P < 0.0001$.

not include an older cohort. If this cohort is not included (6 subjects) neither scanner identified a significant correlation between age and radiodensity in this data set (scanner 1: Pearson $r = -0.224$, $P = .210$).

Contrast-enhanced MRI has become a universal standard in the evaluation of MS such that the majority of patients with MS have had multiple gadolinium-enhanced brain MRI. Recently it has been shown that trace gadolinium is retained in the brain (13, 14). Although the quantity of retained gadolinium is small and retained gadolinium considered to be localized to discrete brain nuclei, we investigated whether retained gadolinium could impact the measured radiodensity of the brain. Previous studies report accumulation of gadolinium in the basal ganglia and dentate nucleus, which increases with numbers of gadolinium exposures. We found no correlation between total brain radiodensity and the numbers of prior gadolinium-enhanced brain MRIs in our data set (see online supplemental Figure S1). We also found that patients with small numbers of gadolinium studies (≤2) maintained a higher brain radiodensity than control subjects. The pool of patients with MS with low numbers of gadolinium-enhanced scans (≤2 gadolinium exposures, 25 cases) was compared with 25 random cases from the control population; the mean difference in brain radiodensity measured at 2.8 HU, and the difference remained significant ($P < .0001$).

Histogram analysis of the control subjects and the total group of MS patients and the three patient cohorts based on

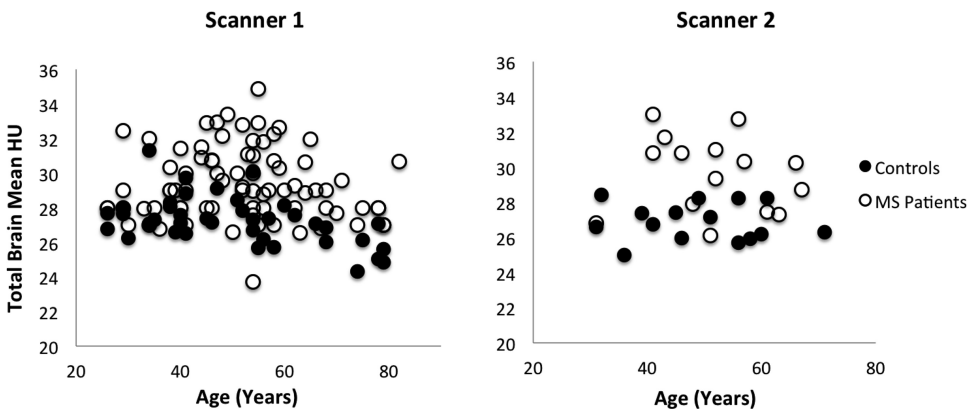

Figure 4. Distribution of mean total brain tissue radiodensity as a function of age (scanner 1, left) and (scanner 2, right). The average difference in radiodensity between patients with MS and control subjects was 3.06 HU (11.2%, $P < .0001$) from scanner 1 and 2.71 HU (10.1%, $P < .0001$) for scanner 2. Scanner 2 showed a similar profile (right). Difference between mean radiodensities for all cases (scanner 1, n = 78; scanner 2, n = 30) was not significant, $P = .33$.

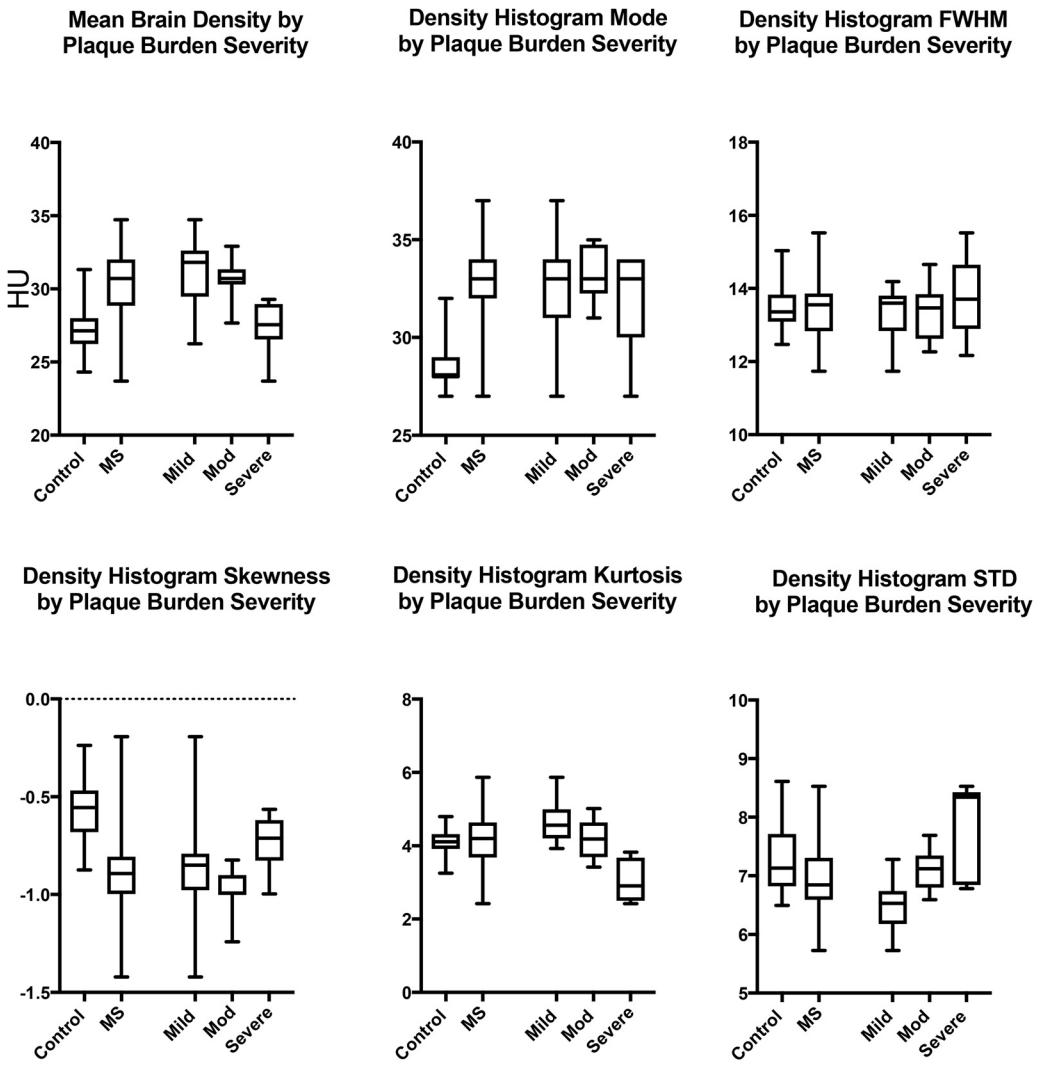

Figure 5. Box and whiskers plots of histogram parameters, scanner 1. FWHM: full-width at half-maximum; STD: standard deviation. The statistics for these plots are summarized in Table 3.

plaque burden seen on MRI was performed (Figure 4). Box and whiskers plot of the histogram metrics for Figure 4 are shown in Figure 5, and accompanying statistics in Table 3. Kruskal-Wallis H test was used with a significance at $P < .05$.

Table 3 shows the statistical significance of the differences in the histogram metrics. Statistically significant differences were found between the control group histogram and the MS group histograms. Further analysis according to plaque burden shows a second trend, with decreasing mean density and decreasing kurtosis from mild to severe plaque burden, with increasing histogram standard deviation with increasing plaque burden.

The ROC curve analysis for mean and mode of the histogram density, histogram skewness, histogram kurtosis, and histogram standard deviation between the total group of patients with MS from scanner 1 (N = 39) and control subjects is shown in Figure 6. The sensitivity, specificity, and area under the ROC curve (AUC) are detailed in Table 4. The AUC analysis in differentiating between MS patients and the control group was good (>0.80) for mean density (0.853), density histogram mode (0.909), and histogram skewness (0.88); fair/poor (0.70–0.80) for STD (0.755); and poor (<0.70) for kurtosis (0.556) (15). Both sensitivity and specificity was the highest for the histogram mode, with diagnostic accuracy being slightly higher than for histogram skewness or mean radiodensity.

When the MS population was limited to patients with only mild lesion load (N = 16), the OC curves were similar (see online supplemental Figure S2). For mild plaque burden, the AUC analysis was good for mean density, mode, and skewness (>0.80) and poor for kurtosis and standard deviation (<0.70). Sensitivity and specificity were the highest for the mean and modal histogram density (AUC = 0.875).

To learn if the radiodensity changes associated with MS could be localized to a particular brain region, CT images were

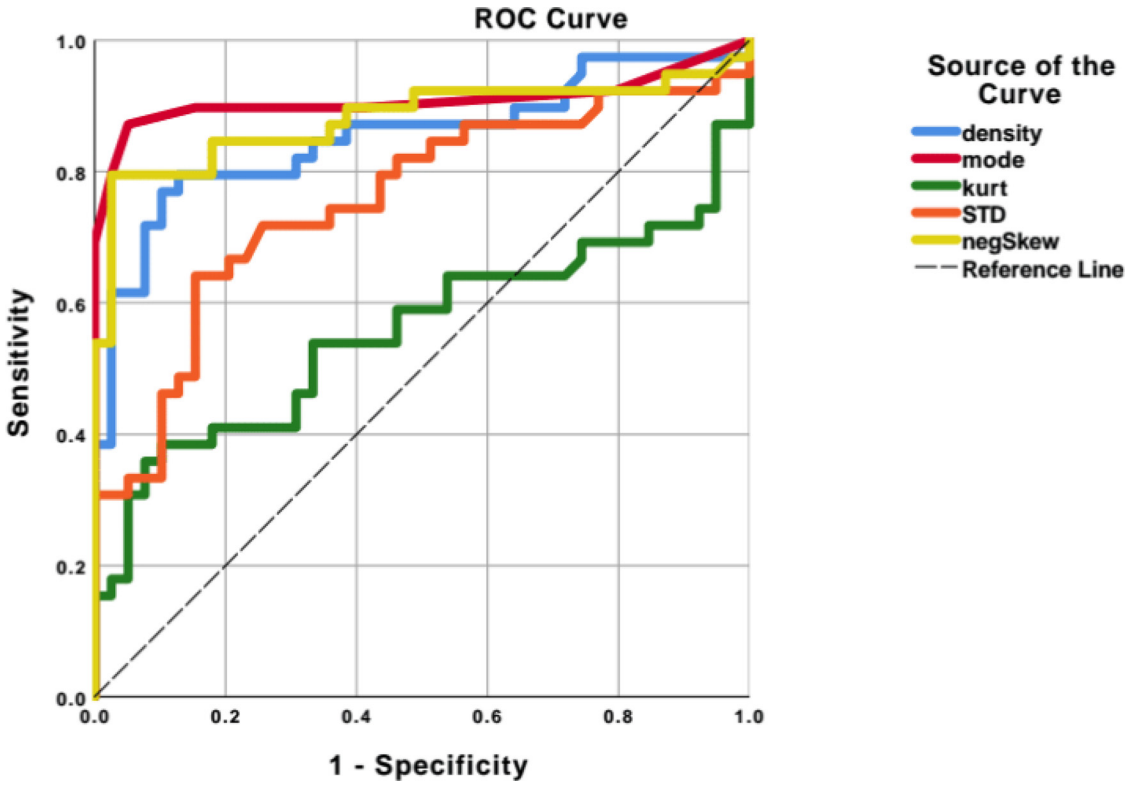

Figure 6. Receiver operating characteristic (ROC) curves for the total MS population from scanner 1. The curve sensitivities and specificities are reported in Table 4. For the total pool of patients with MS from scanner 1 versus the control population, AUC = 0.909 for the histogram mode, regarded as a "good" discriminant (>0.80).

segmented using the reference image MNI152 structural probability map (Figure 7) and the statistics are shown in Table 5. The overall pattern of tissue density across the lobar segmentations is similar, with the largest differences between control subjects and mild MS, with density of MS brain becoming less with increasing plaque burden. Segments of the MNI 152 map are gray matter or favor cortical gray matter, where the 10th segment is white matter alone, and both gray and white matter follow the same patterns of density correlation with disease and plaque severity. Within segments when comparing the total MS population to control subjects, higher levels of significance are seen in the temporal lobe ($P = .0001$), occipital lobe ($P = .0004$), and putamen ($P = .0002$), and no significant difference in the parietal lobe ($P = .9910$), although differences are apparent between the subgoups of MS severity in all the brain segments.

Table 4. ROC Curve Results

Parameter	Sensitivity (%)	Specificity (%)	AUC
Total MS (n = 37)			
Mean	79.5	87.2	0.853
Mode	89.7	84.6	0.909
Skewness	84.6	82.1	0.880
Kurtosis	56.4	53.8	0.556
STD	74.4	64.1	0.654
Mild plaque burden (n = 16)			
Mean	81.3	93.7	0.875
Mode	81.3	100.0	0.850
Skewness	81.3	93.7	0.801
Kurtosis	81.3	62.5	0.789

DISCUSSION

One argument against the use of CT imaging is the exposure to ionizing radiation, as there are documented risks of cancer in association with radiation exposure. The use of CT is always a risk–benefit analysis. We know the risks are very small, which is why CT remains first-line for emergency imaging. But in diseases such as MS, we do not yet know the benefit of the information that quantitative CT can yield. Retrospective research on previously acquired imaging studies would appear a logical place to initiate this investigation.

Studies discussing CT imaging findings in MS have focused on the appearance of MS plaques, and these largely predate the wide use of MR imaging (16-18). To the best of our knowledge, this is the first study to investigate the brain tissue changes of MS by quantitative, digital analysis of CT images. Our study makes several observations: global brain changes of MS can be detected by digital analysis of CT images, seen most clearly as

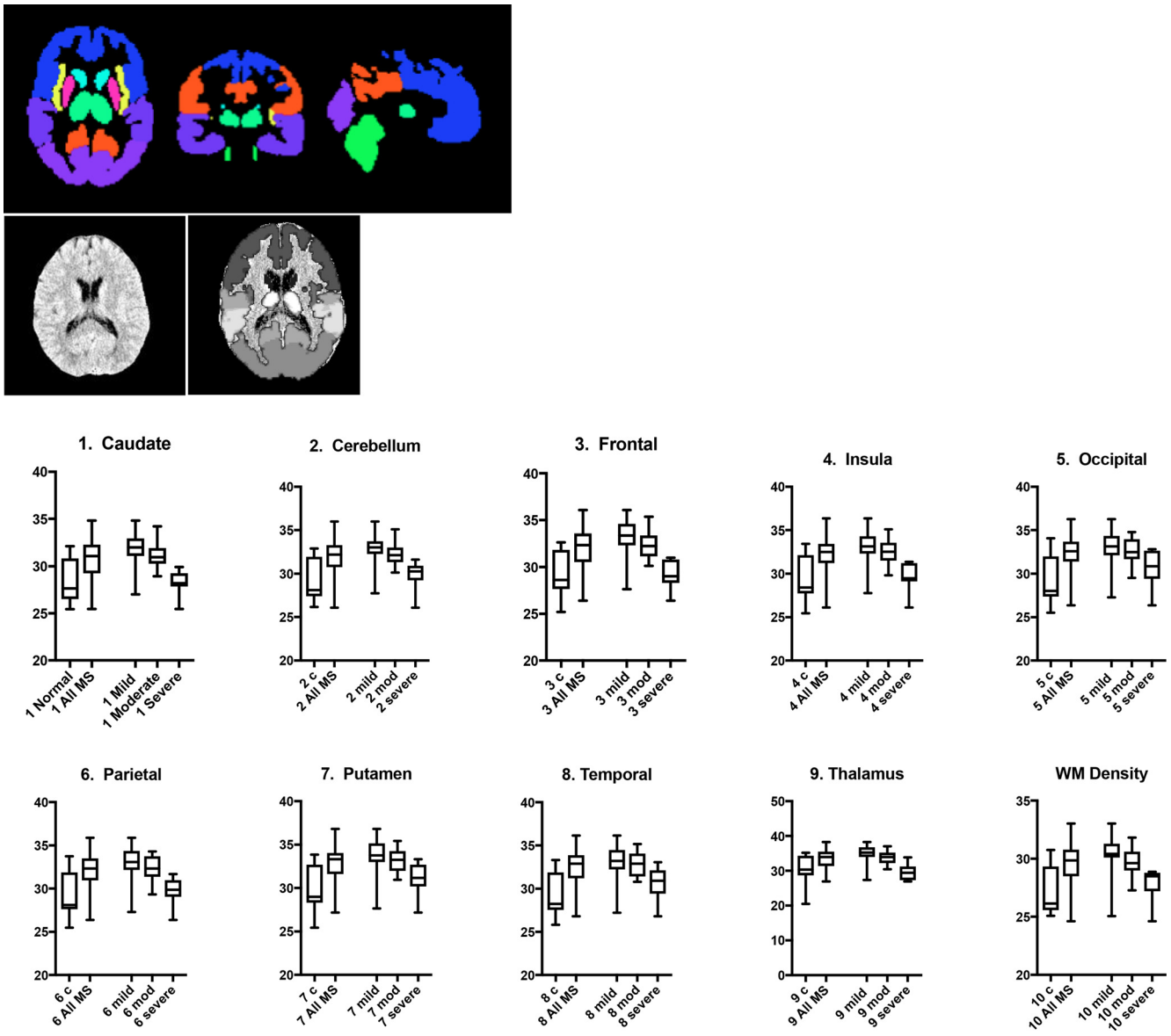

Figure 7. The MNI 152 structural atlas (top) and head CT with coregistered MNI structural atlas. Box and whiskers plots of segmented areas (cases from scanner 1).

changes in the overall brain radiodensity. Significant differences between histograms of MS patients and control subjects are reflected in differences in histogram mean, mode, skewness, kurtosis, and standard deviation. Differences between control subjects and patients with MS are significant even in the MS cases with little visible plaque burden, as seen on routine diagnostic MRI scans.

The CT histogram of MS brain measures changes in NABT as evidenced by 2 observations. First, a shift of the group histogram mode (Figures 1 and 3) indicates a change to a large volume of brain tissue, larger than the plaque volume in most cases. Second, the various histogram metrics correlate only indirectly with plaque burden. The difference in histogram mean density between patients with MS and control subjects is greater when the plaque burden is less, and the difference decreases with increasing plaque burden. These observations suggest 2 opposing phenomena in terms of radiodensity, one causing higher radiodensity and which does not correlate with plaque burden, and a second causing decreased radiodensity, with correlation to plaque burden. This is consistent with a number of previous studies that characterize global changes in the clinically isolated syndromes, to be followed by the characteristic white matter lesions as the disease progresses.

Gross segmentation of the brain CT images shows that the pattern of radiodensity change is seen throughout the brain, as is the correlation with disease severity, and it does not appear to localize to gray or white matter. As with the total brain findings, the differences are greater in cases of lesser plaque burden, and lesser as the plaque burden increases. This would appear to correlate with the idea that plaques are of lower density, and

Table 5. Regional Brain HU Values as Segmented by the MNI152 Structural Atlas (Figure 7)

	Nml	Mild	Mod		Nml	Mild	Mod
1. Caudate				2. Cerebellum			
All MS	0.0674			All MS	0.0107*		
Mild	0.0066**			Mild	0.0040**		
Mod	0.0696	0.8670		Mod	0.0095**	0.9966	
Severe	0.9249	0.0018**	0.0179*	Severe	0.9999	0.0285*	0.0549
3. Frontal				4. Insula			
All MS	0.0396*			All MS	0.0013**		
Mild	0.0051**			Mild	0.0006***		
Mod	0.0303*	0.9531		Mod	0.0030**	0.9836	
Severe	0.9434	0.0018**	0.0096*	Severe	0.9980	0.0186*	0.0537
5. Occipital				6. Parietal			
All MS	0.0004***			All MS	0.9910		
Mild	0.0006***			Mild	0.0001***		
Mod	0.0007***	0.9996		Mod	0.0005***	0.9907	
Severe	0.7209	0.2321	0.2602	Severe	0.9827	0.0123*	0.0315*
7. Putamen				8. Temporal			
All MS	0.0002***			All MS	0.0001***		
Mild	0.0003***			Mild	0.0003***		
Mod	0.0007***	0.9969		Mod	0.0003***	>0.9999	
Severe	0.6684	0.1588	0.2568	Severe	0.5555	0.2172	0.2323
9. Thalamus				10. White Matter			
All MS	0.0123*			All MS	0.0016**		
Mild	0.0011**			Mild	0.0007***		
Mod	0.0202*	0.8527		Mod	0.0032**	0.9819	
Severe	0.9940	0.0029**	0.0288*	Severe	0.9783	0.0400*	0.1078

Asterisks reflect degree of significance: ns, $P > 0.05$; *$P \leq 0.05$; **$P < 0.01$; ***$P < 0.001$; ****$P < 0.0001$.

plaque accumulation lowers total brain density. More advanced methods of image segmentation may serve to test this hypothesis.

As with MR studies showing signal changes in brain tissue, the actual cause of the change is a topic for speculation, particularly as these are small quantitative global changes. Most studies in MS pathology agree that there is both an inflammatory component and a demyelinating component of the disease, which may occur independently of each other, with the inflammatory process representing a more global phenomenon (19). Our study might suggest that this process correlates with increased radiodensity. Demyelination and plaque formation may correlate with volume loss and the decrease in radiodensity is known to accompany gliosis and plaque formation (18, 20).

The relative novelty of our investigation raises concerns regarding the possible contribution of a covariable to our observations. To this end, the control population has been carefully age- and gender-matched to the MS population to eliminate age and gender as possible confounding variables. To eliminate the possible contribution of differences between scan platforms, data from the two different scan platforms are processed separately. As it might be argued that steroid use could cause an increase in brain radiodensity, the small number of patients using steroids at the time of the CT scan were not included. It might be argued that gadolinium accumulation raises the brain radiodensity; we did not find gadolinium use to contribute significantly to increased total brain radiodensity in our study population. A number of MRI studies have shown changes in the NABT in MS. Our study draws correlation with total brain radiodensity and the MS disease process using the modality of CT.

A growing body of literature suggests iron deposition as a hallmark of the inflammatory process. MS lesions are associated with iron accumulation (21-23) localized to microglia and macrophages (21, 24), which varies with the age of the lesion (21, 24, 25), and iron has been proposed as a biomarker of inflammation in MS (24). Interestingly, iron levels are higher in acute and subacute lesions, but return to the levels of NAWM in chronic lesions (21, 24, 25), supporting the idea that inflammation of MS diminishes in the chronic phases of the disease. Iron and other components of inflammation may be causal to the increased radiodensity seen in less progressed disease, with normalization of radiodensity as inflammation decreases.

Where CT images are of relatively low contrast, tools for digital image analysis are becoming widely available, and CT imaging is highly amenable to quantitative digital image

analysis. Using similar methods described here, we recently investigated the changes which occur in normal early postnatal brain development [26]. We chose MS as a target disease, as it is known that MS involves global changes to brain tissue. The data evidence that the global changes of MS can be detected with quantitative CT image analysis and support the hypothesis that digital analysis of CT images can yield information not evident at routine clinical imaging. Although the lesions of MS are readily apparent on MRI, MS remains a clinical diagnosis and patients with MS may have no obvious brain or spine lesions (27), and lesions of MS can be nonspecific, raising a broad differential diagnosis (27, 28). In addition, patients may not have access to MRI or have a contraindication for MRI. Finally, digital CT methods are highly quantitative, amenable to automation, and with the ability to measure a tissue parameter (tissue density) with increasing accuracy. As such, the role of quantitative CT data in the analysis of brain pathology is a topic for future investigation.

Supplemental Materials

Supplemental Materials: http://dx.doi.org/10.18383/j.tom.2018.00050.sup.01

ACKNOWLEDGMENTS

The work was supported by Geisinger Clinical Research Fund, award SRC-L-58.

Disclosures: No disclosures to report.

Conflict of Interest: The authors have no conflict of interest to declare.

REFERENCES

1. Castriota Scanderbeg A, Tomaiuolo F, Sabatini U, Nocentini U, Grasso MG, Caltagirone C. Demyelinating plaques in relapsing-remitting and secondary-progressive multiple sclerosis: assessment with diffusion MR imaging. AJNR Am J Neuroradiol. 2000;21:862–868.
2. Cercignani M, Bozzali M, Iannucci G, Comi G, Filippi M. Magnetisation transfer ratio and mean diffusivity of normal appearing white and grey matter from patients with multiple sclerosis. J Neurol Neurosurg Psychiatry. 2001;70:311–317.
3. Grenier D, Pelletier D, Normandeau M, Newitt D, Nelson S, Goodkin DE, Majumdar S. T2 relaxation time histograms in multiple sclerosis. Magn Reson Imaging. 2002;20:733–741.
4. Griffin CM, Dehmeshki J, Chard DT, Parker GJ, Barker GJ, Thompson AJ, Miller DH. T1 histograms of normal-appearing brain tissue are abnormal in early relapsing-remitting multiple sclerosis. Mult Scler. 2002;8:211–216.
5. Manfredonia F, Ciccarelli O, Khaleeli Z, Tozer DJ, Sastre-Garriga J, Miller DH, Thompson AJ. Normal-appearing brain t1 relaxation time predicts disability in early primary progressive multiple sclerosis. Arch Neurol. 2007;64:411–415.
6. Yu CS, Lin FC, Liu Y, Duan Y, Lei H, Li KC. Histogram analysis of diffusion measures in clinically isolated syndromes and relapsing-remitting multiple sclerosis. Eur J Radiol. 2008;68:328–334.
7. Edwards MK, Farlow MR, Stevens JC. Multiple sclerosis: MRI and clinical correlation. AJR Am J Roentgenol. 1986;147:571–574.
8. Zhang Y, Brady M, Smith S. Segmentation of brain MR images through a hidden Markov random field model and the expectation-maximization algorithm. IEEE Trans Med Imaging. 2001;20:45–57.
9. Jenkinson M, Beckmann CF, Behrens TE, Woolrich MW, Smith SM. FSL. Neuroimage. 2012;62:782–790.
10. Muschelli J, Ullman NL, Mould WA, Vespa P, Hanley DF, Crainiceanu CM. Validated automatic brain extraction of head CT images. Neuroimage. 2015;114:379–385.
11. Cauley KA, Och J, Yorks PJ, Fielden SW. Automated segmentation of head computed tomography images using FSL. J Comput Assist Tomogr. 2018;42:104–110.
12. Kurtzke JF. Rating neurologic impairment in multiple sclerosis: an expanded disability status scale (EDSS). Neurology. 1983;33:1444–1452.
13. Kanda T, Ishii K, Kawaguchi H, Kitajima K, Takenaka D. High signal intensity in the dentate nucleus and globus pallidus on unenhanced T1-weighted MR images: relationship with increasing cumulative dose of a gadolinium-based contrast material. Radiology. 2014;270:834–841.
14. McDonald RJ, McDonald JS, Kallmes DF, Jentoft ME, Murray DL, Thielen KR, Williamson EE, Eckel LJ. Intracranial gadolinium deposition after contrast-enhanced MR imaging. Radiology. 2015;275:772–782.
15. The Area Under an ROC curve. Available from: http://gim.unmc.edu/dxtests/roc3.htm.
16. Gize RW, Mishkin FS. Brain scans in multiple sclerosis. Radiology. 1970;97:297–299.
17. Gyldensted C. Computer tomography of the brain in multiple sclerosis. A radiological study of 110 patients with special reference to demonstration of cerebral plaques. Acta Neurol Scand. 1976;53:386–389.
18. Weinstein MA, Lederman RJ, Rothner AD, Duchesneau PM, Norman D. Interval computed tomography in multiple sclerosis. Radiology. 1978;129:689–694.
19. Lassmann H. The pathology of multiple sclerosis and its evolution. Philos Trans R Soc Lond B Biol Sci. 1999;354:1635–1640.
20. Phillips MD, Grossman RI, Miki Y, Wei L, Kolson DL, van Buchem MA, Polansky M, McGowan JC, Udupa JK. Comparison of T2 lesion volume and magnetization transfer ratio histogram analysis and of atrophy and measures of lesion burden in patients with multiple sclerosis. AJNR Am J Neuroradiol. 1998;19:1055–1060.
21. Chen W, Gauthier SA, Gupta A, Comunale J, Liu T, Wang S, Pei M, Pitt D, Wang Y. Quantitative susceptibility mapping of multiple sclerosis lesions at various ages. Radiology. 2014;271:183–192.
22. Hagemeier J, Weinstock-Guttman B, Bergsland N, Heininen-Brown M, Carl E, Kennedy C, Magnano C, Hojnacki D, Dwyer MG, Zivadinov R. Iron deposition on SWI-filtered phase in the subcortical deep gray matter of patients with clinically isolated syndrome may precede structure-specific atrophy. AJNR Am J Neuroradiol. 2012;33:1596–1601.
23. Stankiewicz JM, Neema M, Ceccarelli A. Iron and multiple sclerosis. Neurobiol Aging. 2014;35 *Suppl* 2:S51–S58.
24. Mehta V, Pei W, Yang G, Li S, Swamy E, Boster A, Schmalbrock P, Pitt D. Iron is a sensitive biomarker for inflammation in multiple sclerosis lesions. PLoS One. 2013;8:e57573.
25. Bagnato F, Hametner S, Yao B, van Gelderen P, Merkle H, Cantor FK, Lassmann H, Duyn JH. Tracking iron in multiple sclerosis: a combined imaging and histopathological study at 7 Tesla. Brain. 2011;134(Pt 12):3602–3615.
26. Cauley KA, Hu Y, Och J, Yorks PJ, Fielden SW. Modeling early postnatal brain growth and development with CT: Changes in the brain radiodensity histogram from birth to 2 Years. AJNR Am J Neuroradiol. 2018;39:775–781.
27. Fazekas F, Barkhof F, Filippi M, Grossman RI, Li DK, McDonald WI, McFarland HF, Paty DW, Simon JH, Wolinsky JS, Miller DH. The contribution of magnetic resonance imaging to the diagnosis of multiple sclerosis. Neurology. 1999;53:448–456.
28. Traboulsee AL, Li DK. The role of MRI in the diagnosis of multiple sclerosis. Adv Neurol. 2006;98:125–146.